A theoretical and experimental study of the effects of NaCl and the competitive chemisorption of ions at the surface sites in the context of galena flotation

Anna M. Nowosielska†, Aleksandar N. Nikoloski† and Drew F. Parsons*‡

†College of Science, Health, Engineering and Education, Murdoch University, 90 South St, Murdoch, WA 6150, ***Australia***

‡Department of Chemical and Geological Sciences, University of Cagliari, Cittadella Universitaria, 09042 Monserrato, CA, ***Italy***

Keywords: Flotation, Galena, Bubble, Zeta potential, Chemisorption

Main Findings:

- The recovery of galena improves as a result of NaCl addition.
- Our galena surface complexation model is a "two-site / not amphoteric" model.
- The theoretical predictions of the models support the experimental results.
- The decreasing repulsion at higher ionic strengths corresponds to a higher galena recovery.

*Electronic mail: drew.parsons@unica.it

GRAPHICAL ABSTRACT

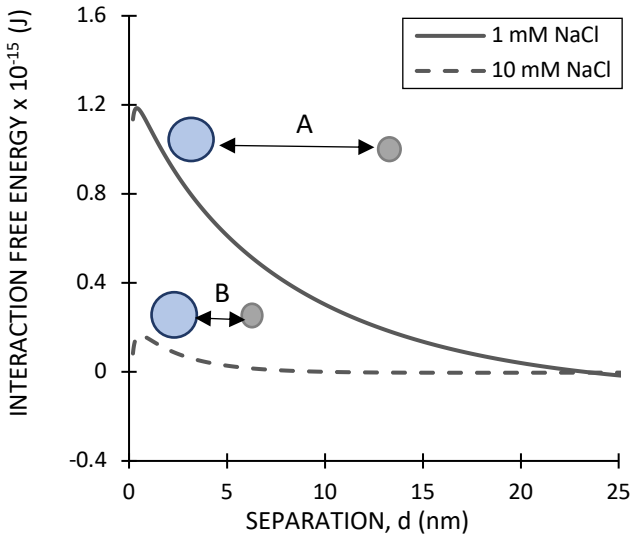

A: Lower ionic strength

↑ repulsion

↑ particle-bubble separation

↓ recovery

B: Higher ionic strength

↓ repulsion

↓ particle-bubble separation

↑ recovery

ABSTRACT

In this study we have investigated the effects of increasing the NaCl concentration on the flotation of galena. Experiments were carried out using a Hallimond tube in NaCl solutions with concentrations of 1, 10 and 100 mM, at pH 9. It was found that the recovery of galena improved for higher NaCl concentrations.

Zeta potential measurements made on galena particles conditioned in NaCl solutions were used to calibrate the parameters for describing a chemisorption model representing charge regulation at the galena binding sites. Our galena chemisorption model presented here is a "two-site/not amphoteric" surface complexation model. A chemisorption model representing the charge regulation process on the surface of an air bubble has also been applied. The zeta potentials calculated using these models were in agreement with the measured values, indicating that these models can be applied to predict the potentials on the surface of galena and an air bubble for a range of NaCl concentrations and pH.

In order to investigate the mechanisms of particle-bubble interactions for each NaCl concentration, the total interaction free energy as a function of the separation distance between galena and an air bubble was determined. It was found that at a NaCl concentration of 1 mM, due to adsorption of ions at the galena surface, repulsion dominated the interaction and the lowest galena recovery was reported. With an increase in NaCl concentration in solution to 100 mM, the total interaction between galena and an air bubble was represented by a purely attractive total interaction free energy curve. The theoretical predictions of the models supported the experimental results, with a stronger attraction predicted by the models at higher ionic concentrations, corresponding to a higher galena recovery during flotation.

1. INTRODUCTION

Froth flotation is one of the most successful and efficient techniques used in the mineral industry for separating minerals from gangue. The process involves adding mineral particles to a solution to form an aqueous pulp and aerating this with air bubbles, which results in the formation of a particle-bubble aggregate that can rise to the surface of the pulp. The selectivity of the process has been shown to strongly depend on control of the surface forces involved in the interactions (Pineres and Barraza,2011). The thinning and rupture of the intervening water film between a particle and an air bubble, which is necessary for a successful attachment, is mainly controlled by the surface forces. In order to predict the flotation behaviour, many investigations have focused on understanding of these surface forces during the interaction.

The DLVO theory, named after Derjaguin and Landau (1941), Verwey and Overbeek (1948), formulates the classical theory of colloidal dispersions. This theory incorporates two components - the attractive van der Waals force and the repulsive ionic diffuse layer force. The magnitude of the van der Waals force is governed by a Hamaker constant calculated for the interaction and is expressed in terms of the separation distance between the two interacting objects. The ionic diffuse layer force, on the other hand, is determined by the surface chemistry and therefore will be significantly affected by any changes to the surface potential or the electrolyte concentration. This work studies the effects of the ionic concentration in froth flotation of galena, therefore, understanding the contribution from the ionic diffuse layer force is an important objective.

This is important as, due to the scarcity of fresh water, more flotation plants around the world are looking into utilising seawater or recycled water for mineral processing. Using water which contains high electrolyte concentrations can be beneficial to mineral recovery. However, the process becomes more complex, mainly due to the differences in chemistry between salt water and fresh water. The mechanisms involved in the process are still not well understood, underlining the need for further research.

A number of studies have reported that high electrolyte concentration in water has a positive effect on mineral recovery (Castro et al.,2013; Hencer et al.,2001; Lucay et al.,2015; Ramos et al.,2013; Smith and Heyes,2012). This has been mainly attributed to increased particle-bubble

attachment efficiency and a decreased bubble coalescence. The increased attachment efficiency has also been linked to a reduction of particle and bubble zeta potentials, resulting from the compression of the ionic diffuse layers at higher electrolyte concentrations.

The aim of this study was to explore the effects of NaCl concentration on the flotation of galena. We measured the recovery of galena by micro-flotation experiments at different ionic concentrations. Here we present a theoretical investigation of the galena/air bubble interactions for the different NaCl concentrations, supported by the experimental measurements of galena zeta potentials.

2. EXPERIMENTAL

2.1 Minerals and Reagents

The mineral tested was galena (>99% PbS). The galena specimen was from an unknown location. Deionised water was used in all experiments. Analytical grade sodium chloride (NaCl) was used in each test. Analytical grade sodium hydroxide (NaOH) was used to regulate the pH. The particle size distribution for the galena feed was determined by laser diffraction (Microtrac S3500) and is depicted in Figure 2. The results indicate that P_{80} of the galena sample was 80µm. Figure 3 shows the Scanning Electron Microscopy/Energy Dispersive X-ray Spectroscopy (SEM/EDX) analysis of the feed material.

2.2 Zeta Potential Measurements and the Chemisorption Models for Galena and Air Bubble

The zeta potentials of galena dispersed in 0.5, 1, 5, 10 and 100 mM NaCl solutions were measured using a Malvern Nano-ZS90 zeta potential analyser (Malvern Instruments, UK) at room temperature. All electrophoretic mobility results obtained were converted to zeta potential values using the Smoluchowski equation. The measurements involved the freshly ground galena particles (~ 5µm) distributed in either 0.5, 1, 5, 10 or 100 mM NaCl background solution, at a pH range of 2-10. At least 3 measurements were done at each condition, with the

average values plotted in Figure 4. Figure 4 also illustrates the zeta potentials of galena calculated using a chemisorption model describing competitive ion binding at the galena surface. This model is represented by Eq.(1-4).

According to the galena chemisorption model, there are two separate binding sites on the surface of galena where the dissociation reactions take place, represented as: (1) - a negative galena site $\mathrm{X^-}$ (neutral when $\mathrm{H^+}$ is bound):

$$\mathrm{XH} \overset{\mathrm{pK_{H_1}}}{\Longleftrightarrow} \mathrm{X^-} + \mathrm{H^+} \tag{1}$$

$$\mathrm{XNa} \overset{\mathrm{pK_{Na}}}{\Longleftrightarrow} \mathrm{X^-} + \mathrm{Na^+} \tag{2}$$

and, (2) - a neutral galena site X (positive when $\mathrm{H^+}$ is bound):

$$\mathrm{XH^+} \overset{\mathrm{pK_{H_2}}}{\Longleftrightarrow} \mathrm{X} + \mathrm{H^+} \tag{3}$$

$$\mathrm{XCl^-} \overset{\mathrm{pK_{Cl}}}{\Longleftrightarrow} \mathrm{X} + \mathrm{Cl^-} \tag{4}$$

For a pH higher than the isoelectric point, the surface of galena will be negatively charged, which is attributed to the number of dissociated type-1 sulfur sites. The neutral sites result from positively charged lead and lead hydroxides ions adsorbing at the Stern layer onto the sulfide sites (Fornasiero et al.,1993).

At the type-1 negative galena sites, protons $(\mathrm{H^+})$ compete with sodium $(\mathrm{Na^+})$ cations to bind directly onto the site. At the type-2 neutral galena sites, protons $(\mathrm{H^+})$ compete with chloride $(\mathrm{Cl^-})$ anions. In this model there is only single-binding of ions at each of the sites. Previous galena chemisorption model applied by Fornasiero et al.,1993 only considered a single galena site where the competitive ion binding is taking place, however, we found the two-site model presented here to be better at quantitatively predicting galena zeta potentials based on the measured zeta potentials.

For the purpose of illustrating the competitive ion binding on the surface of an air bubble, we have applied a double-layer model of the air bubble/water interface from a study of Leroy et al.,2012, which can be represented by Eq.(5-7). By using the measured zeta potentials of an air bubble in various NaCl concentration from the works of Yang et al.,2001 we attempted to

optimise the model parameters in order to predict the zeta potential values at a given ionic concentration and pH. Figure 5 depicts the measured and calculated zeta potentials of an air bubble in various NaCl concentrations against pH.

The dissociation reactions taking place at a site on an air bubble surface are as follows:

$$XH \overset{pK_H}{\Longleftrightarrow} X^- + H^+ \tag{5}$$

$$XH_2{}^+ \overset{pK_{HH}}{\Longleftrightarrow} XH + H^+ \tag{6}$$

In this study the bubble model is being applied at low ionic concentrations of 1 mM and 10 mM and according to Leroy et al.,2012, at these concentrations it will be the chloride anion and not the sodium cation which is able to come closer to the surface. Keeping this in mind, the model includes the following reaction representing the adsorption of chloride (Cl^-) on the bubble surface:

$$XH - Cl^- \overset{pK_{HCl}}{\Longleftrightarrow} XH + Cl^- \tag{7}$$

The surface complexation model for an air bubble in Eq.(5-7) is an amphoteric "one-site/two pK" model. The model indicates a bubble site that is negatively charged (X^-) , where either the single binding of protons (H^+) Eq.(5), the double-binding of protons (H^+) Eq.(6) or the double-binding of the Cl^- ions Eq.(7) can take place. The H^+ ions compete with the Cl^- ions during the double-binding process.

The terms pK_{H_1}, pK_{H_2} and pK_H are the equilibrium constants associated with the surface adsorption of protons. In this study the equilibrium constants for the adsorption and desorption reactions of all ions were determined by least-square fitting to the measured zeta potential values for the different ionic concentrations.

The total surface charge (σ_s) for a given site can be calculated according to:

$$\sigma_s = q_s N_s + \sum_i q_i \Gamma_i \tag{8}$$

where q_s is the charge of the dissociated site, N_s is the site density (number of sites per unit area) and q_i is the ionic charge (Parsons and Salis,2019).

123 The total amount of bound charge (Γ_i) from ion i can be calculated from:

$$\Gamma_i = \frac{N_s}{A_s}\left[\frac{a_i}{K_i} + \sum_j a_i a_j \left(\frac{1}{K_i K_{ij}} + \frac{1}{K_j K_{ji}}\right)\right] \quad (9)$$

124 where K_i and K_j indicate the single-binding of ion i and j, respectively, K_{ij} represents binding
125 of ion j to a site with ion i already bound, and K_{ji} describes a site with ion i double-binding to
126 a site with ion j already bound.

127 A_s is a measure of the total association or in other terms, an inverse of γ_s (γ_s being a fraction
128 of fully dissociated surface sites) and can be written as:

$$A_s = \frac{1}{\gamma_s} = 1 + \sum_m \frac{a_m}{K_m}\left(1 + \sum_n \frac{a_n}{K_{mn}}\right) \quad (10)$$

129 The term a_i does not describe the surface activity of an ion, rather it corresponds to the "partial
130 ion activity" at a particular concentration, and according to Parsons and Salis,2015 and 2019,
131 is quantified by:

$$a_i = c_i^{bulk} e^{-q_i\psi_0/kT} \quad (11)$$

132 where c_i^{bulk} is the concentration of ion i in the bulk, ψ_0 is the electrostatic potential at the
133 surface, k is the Boltzmann constant (1.3806 x 10^{-23} J/K) and T is the temperature (298 K).

TABLE 1. Parameters used to fit the chemisorption model for galena calibrated using the measured zeta potentials (galena zeta potentials in 10 mM NaCl).

PARAMETER	VALUE
N_s negative (sites m^{-2})	1.519 x 10^{16}
N_s neutral (sites m^{-2})	2.765 x 10^{16}
pK_{H1}	5.265
pK_{H2}	2.393
pK_{Na}	-2.376
pK_{Cl}	7.911

TABLE 2. Parameters used to fit the chemisorption model for an air bubble calibrated using the measured bubble zeta potentials in 10 mM NaCl, taken from Yang et al.,2001.

PARAMETER	VALUE
N_s (sites m^{-2})	4.676 x 10^{16}
pK_H	5.812
pK_{HH}	2.984
pK_{HCl}	1.962

The model parameters presented in Table 2 are in good agreement with the ones reported by Leroy et al.,2012 ($\mathbf{pK_H}$ = 5.06, $\mathbf{pK_{HH}}$ = 2.54, $\mathbf{pK_{HCl}}$ = 1.8). The value of the site density $(\mathbf{N_s})$, however, is in one order of magnitude lower than the value reported by Leroy et al., 2012 ($\mathbf{N_s}$ = 3.8 x 10^{17} sites m^{-2}). In their calculations, these authors assumed that the electrical potential at the outer Helmholtz plane is equal to the zeta potential, indicating that the slipping plane is located at the outer Helmholtz plane of the diffuse layer at the gas/water interface, hence possible discrepancies in the parameter values obtained.

2.3 Micro-Flotation Experiments

The micro-flotation tests of the dispersed galena were performed in a Hallimond tube with air as the bubble source. Shortly prior to the experiments a small amount of the feed was dry-ground using a ceramic mortar and pestle. After each experiment, the galena feed was stored in a freezer to reduce oxidation. Each micro-flotation experiment consisted of 2 grams of galena particles suspended in 250 mL of test solution. The test solution was prepared using the deionised water and contained either 1, 10 or 100 mM NaCl. The pH was adjusted to 9 using NaOH. This pulp was then transferred to a Hallimond tube, agitated and conditioned for 3 minutes. It was aerated for 1, 3 and 7 minutes with air at a flow rate of 60 mL/min. The froth concentrates and the tailings were recovered and weighed after filtration and drying. For each test the recovery of galena was calculated by dividing the mass of the froth concentrate by the combined mass of the froth concentrate and the tailings and is presented as a percentage of

recovery. Any mass of the salt precipitation after drying was not included in the recovery calculations, as it was assumed insignificant at the 1 and 10 mM NaCl concentrations. After filtration, the concentrates and the tailings from the 100 mM experiments were washed using deionised water to remove any possible salt from the solid samples once dried. For this reason, at the 100 mM NaCl concentration, all the salt was assumed to be washed out of the samples, hence, was not considered in the galena recovery calculations.

2.4 Total Interaction Free Energy and the DLVO Theory

The DLVO theory describes the total interaction energy between two objects in terms of a balance of the attractive and repulsive contributions to the total free energy. However, for NaCl concentrations higher than 100 mM, the ionic diffuse layer force is screened, leaving the van der Waals force as the dominant factor in the interaction. The total interaction free energy $(\mathbf{F_{tot}})$ can be broken down into four individual contributions:

$$\mathbf{F_{tot} = F_{el} + F_{en} + F_{vdW} + F_{chem}} \qquad (12)$$

$\mathbf{F_{el}}$ represents the direct electrostatic energy due to surface and electrolyte charges, $\mathbf{F_{en}}$ is the contribution due to the entropy (osmotic energy) of ions physisorbed near the surface. The term $\mathbf{F_{vdW}}$ represents the van der Waals interactions characterised by the Hamaker constant for the system and $\mathbf{F_{chem}}$ is the chemisorption free energy resulting from ion binding (Parsons and Salis,2019), also known as charge regulation. The electrostatic energy $\mathbf{F_{el}}$ is determined by the electrostatic potential $\boldsymbol{\psi(z)}$ generated by physisorbed ions (the so-called electric double layer) and by the surface charge (Eq.8), where $\mathbf{z}$ is the position of the ion (its distance from the galena surface) (Parsons and Ninham,2012):

$$\mathbf{F_{el}} = \frac{\boldsymbol{\varepsilon_0 \varepsilon}}{2} \int_0^{\mathbf{L}} \left(\frac{\mathbf{d\psi}}{\mathbf{dz}}\right)^2 \mathbf{dz} \qquad (13)$$

and $\mathbf{L}$ represents the separation distance between the two interacting surfaces.

The entropic energy $\mathbf{F_{en}}$is generated by the concentration profiles $\mathbf{c_i(z)}$ of the adsorbed ions, according to the following:

$$F_{en} = kT\sum_{i}\int_{0}^{L} dz\left\{c_i(z)\ln\frac{c_i(z)}{c_{i0}} - c_i(z) + c_{i0}\right\} \quad (14)$$

where c_{i0} is the bulk activity of ion i (Parsons and Ninham,2012). A more detailed description of the term F_{chem} from Eq.(12) can be found in the studies of Parsons and Salis,2015 and 2019.

While the chemisorption contributions to the total free energy are mainly influenced by the surface charge and the concentration and distribution of ions in the system, the non-electrostatic van der Waals interactions F_{vdW} are characterised by a Hamaker constant (A_{132}), with

$$F_{vdW} = \frac{-A_{132}}{12\pi d^2} \quad (15)$$

The Hamaker constant characterises the interaction between sphere 1 (particle) and sphere 2 (air bubble) immersed in aqueous medium 3 (aqueous solution). Using Lifshitz theory, the Hamaker constant can be calculated from the frequency dependent dielectric properties (optical spectra) of the continuous phases (Lee et al.,2002; Bergström,1997). The non-retarded Hamaker constant (A_{132}) for galena (1) and a bubble (2) interacting in an aqueous solution (3) can be approximated as:

$$A_{132} = \frac{3kT}{2}\sum_{n=0}^{\infty}{}'\sum_{s=1}^{\infty}\frac{(\Delta_{13}\Delta_{23})^s}{s^3} \quad (16)$$

The prime on the first summation indicates that when n=0 (the static contribution) the value is multiplied by 0.5 (Takagishi et al.,2019).

The quantity in Eq.(16) is a reflection coefficient, defined as:

$$\Delta_{kl} = \frac{\varepsilon_k(i\zeta_m) - \varepsilon_l(i\zeta_m)}{\varepsilon_k(i\zeta_m) + \varepsilon_l(i\zeta_m)} \quad (17)$$

which describes the difference in the dielectric response function of material k and l, respectively. In Lifshitz theory, it is evaluated at the imaginary frequency $(i\zeta_m)$, where

$$\zeta_m = m\frac{4\pi^2 kT}{h} \quad (18)$$

Here $\mathbf{h}$ is the Planck constant (6.626 x 10^{-34} J/K), $\mathbf{k}$ is the Boltzmann constant, $\mathbf{m}$ is an integer (0,1,2,3,4…) and $\mathbf{T}$ is the absolute temperature. At room temperature, $\boldsymbol{\zeta_m}$ are sampled at integral multiples of 2.4 x 10^{14} rad/s.

We apply a model for the dielectric function of galena provided by Bergström,1997, using

$$\varepsilon(i\zeta_m) = 1 + \frac{C_{UV}}{1 + \left(\frac{\zeta_m}{\omega_{UV}}\right)^2} + \frac{C_{IR}}{1 + \left(\frac{\zeta_m}{\omega_{IR}}\right)^2} \tag{19}$$

Optical parameters $\mathbf{C_{UV}}$ and $\mathbf{C_{IR}}$ are the adsorption strengths in the UV and IR range, and for a cubic galena these values are 15.04 and 153, respectively. For a cubic galena, the terms $\boldsymbol{\omega_{UV}}$ and $\boldsymbol{\omega_{IR}}$, which represent the adsorption frequencies in the UV and the IR range, have a value of 0.167 (10^{16} rad/s) and 0.14 (10^{14} rad/s), respectively (Bergström,1997). For water we used Dagastine's numerical data (Dagastine et al.,2000). The dielectric function of air is taken to be simply $\boldsymbol{\varepsilon_{air} = 1}$. In this study, the Hamaker constant for the interaction between galena and an air bubble in water was calculated to be 6.9984 x 10^{-21} J.

This approach provides a numerical calculation of the full total interaction free energy including charge regulation, and contrasts with an "approximate" analytical formula commonly used, one which assumes constant potential conditions. In this work we attempted to differentiate between the two methods and the results are shown in Figure 8. Generally speaking, the free energy of charge regulation $\boldsymbol{(F_{chem})}$ is the key difference between the two methods and provides stronger repulsion at short-mid range distances of around one Debye length.

The Debye length characterizes the screening distance of the electrostatic force, or in other words, the thickness of the electrical double layer denoted as $\boldsymbol{(\kappa^{-1})}$, and is defined as:

$$\kappa^{-1} = \sqrt{\frac{\varepsilon_r \varepsilon_0 kT}{e^2 \sum_i \rho_i^{\infty} z_i^2}} \tag{20}$$

where $\boldsymbol{\varepsilon_0}$ is the permittivity of free space, $\boldsymbol{\varepsilon_r}$ is the dielectric constant of the medium, $\mathbf{k}$ is the Boltzmann constant, $\mathbf{T}$ is the absolute temperature, $\mathbf{e}$ is the electronic charge, $\boldsymbol{\rho_i}$ is the number density of ion i and $\boldsymbol{z_i}$ is the ion valency. According to Eq.(20), the Debye length will decrease

monotonically as the ion concentration increases and will continue to decrease to a point where no long-range electrostatic forces will be expected in a concentrated electrolyte (Smith et al.,2016).

2.4.1 The Poisson-Boltzmann model

The total free energy, (Eq.12), develops as a result of ion adsorption (the electric double layer) at the surface, forming ion concentration profiles $c_i(z)$. Ions adsorb primarily in response to the electrostatic potential $\psi(z)$. Assuming that each ion is in equilibrium with the bulk solution, the concentration profile is formed as a Boltzmann distribution determined by the electrostatic energy of the ion:

$$c_i(z) = c_{i\infty}\exp\left(-\frac{Z_i e\psi(z)}{kT}\right) \tag{21}$$

where k is the Boltzmann constant, T is the temperature and $c_{i\infty}$ is the bulk number concentration of all of the ions.

The electrostatic potential $\psi(z)$ is determined by the Poisson equation (the first of Maxwell's equations):

$$\frac{d^2}{dz^2}\psi(z) = -\frac{e}{\varepsilon\varepsilon_0}\sum_i Z_i c_{i\infty}\exp\left(-\frac{Z_i e\psi(z)}{kT}\right) \tag{22}$$

where e is the elementary charge and Z_i is the valency of the corresponding ion. ε and ε_0 are the dielectric constant of the medium and the permittivity of free space. Solving for $c_i(z)$ and $\psi(z)$ simultaneously, Eq.(21) and Eq.(22) together, form the nonlinear Poisson-Boltzmann model.

Solving the Poisson equation Eq.(21), however, requires defining the boundary conditions relating the gradient of the electrostatic potential at the galena and bubble surfaces to their respective surface charges, as follows:

$$\left(\frac{d\psi}{dz^2}\right)_{surface} = \frac{-\sigma}{\varepsilon\varepsilon_0} \tag{23}$$

239 Here we apply the charge regulation model, Eq.(8) to determine the surface charges of the two
240 surfaces.
241 We solve the nonlinear Poisson-Boltzmann model by finite element methods using the FEniCS
242 software (Alnæs et al.,2015). Once $c_i(z)$ and $\psi(z)$ have been calculated, they are used to
243 determine the total interaction free energy Eq.(12), between galena and an air bubble, both
244 represented as flat planes. Finally, the Derjaguin approximation (Derjaguin,1934) is applied to
245 convert the flat-plane interaction energy $F(d)$ into a force $f(d)$ between two spherical
246 particles:

$$f(d) = 2\pi\left(\frac{R_1 R_2}{R_1 + R_2}\right)F(d) \tag{24}$$

247 where R_1 and R_2 are the radii of the two particles (galena particle and air bubble), respectively.
248 Figure 1 illustrates the sequence of steps required to perform the calculations presented in this
249 study.

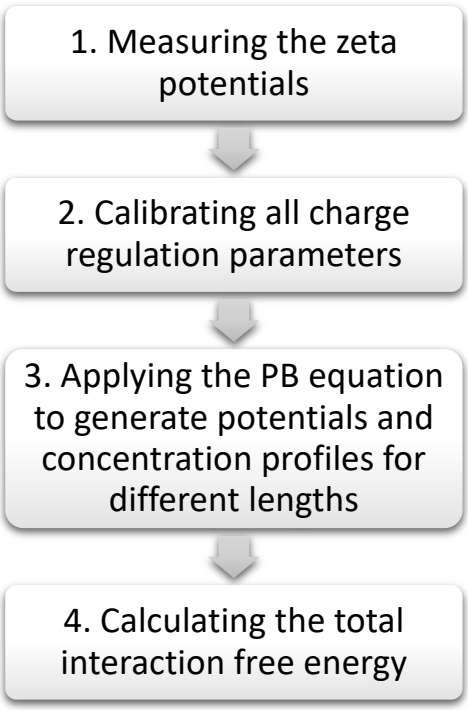

Figure 1. The calculation/optimization sequence implemented in the study.

1. Zeta potentials are measured as a function of pH and the ionic concentration.
2. The measured zeta potentials from Step 1 are used to calibrate the charge regulation parameters of our model, determining the charge-regulated surface charge (σ_s) in Eq.(8). The charge regulation parameters are fitted by least-square difference to minimize the difference between the measured zeta potentials and the surface potentials calculated by the PB model for galena and air bubble surfaces, taken separately.
3. Using the charge regulation parameters from Step 2 and the PB model from Eq.(21) and Eq.(22), the potential and the ion concentration profiles for galena and air bubble interacting at various separation distances (d) are calculated.
4. Using the electrostatic potentials and the ion concentration profiles calculated in Step 3, the total interaction free energy between the two surfaces, separated by distance (d), is calculated using Eq.(12). The total free energy between two flat surfaces is then converted to a force between spherical particles using the Derjaguin approximation Eq.(24).

3. RESULTS AND DISCUSSION

3.1 Particle Size Analysis

Figure 2 shows the particle size distribution of the galena feed. The P_{80}, which represents the size at which 80% of the galena particles are passing was 80µm. For the purpose of calculating the total interaction free energy between a galena particle and an air bubble, 40µm was used as the mean radius of a galena particle and 1000µm was used as the radius of the air bubble.

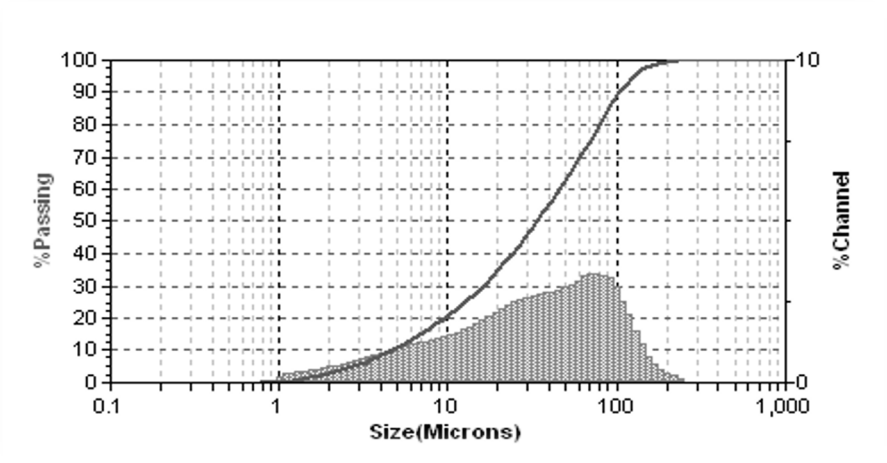

Figure 2. Particle size distribution of the galena feed used in this study.

3.2 SEM/EDX Analysis

SEM/EDX analysis was conducted in order to examine the structural morphology of the galena feed material. The results are presented in Figure 3 below.

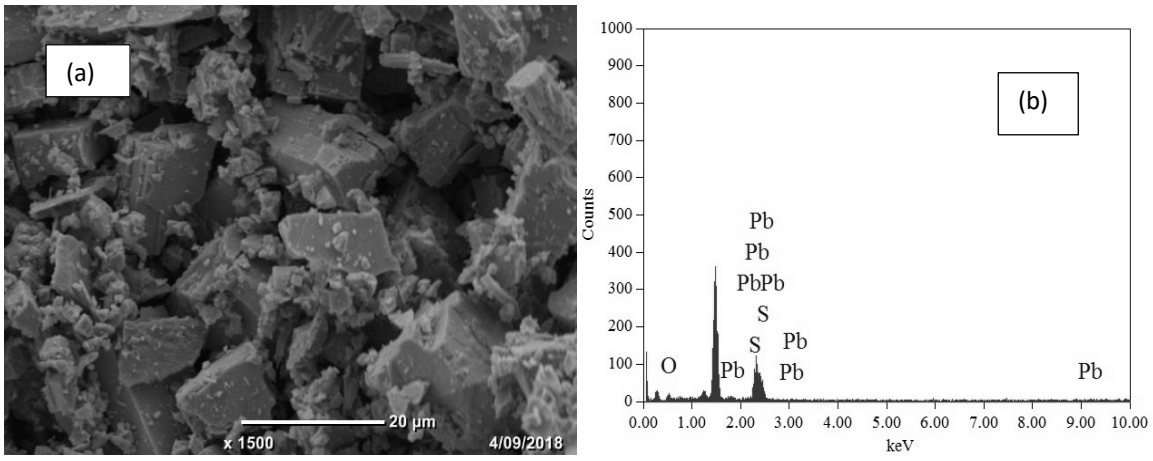

Figure 3. SEM/EDX analysis of galena feed (a) SEM image of galena particles and (b) corresponding EDX spectra for image (a).

The examination of the galena feed material using the SEM (Figure 3 (a)) indicated a presence of particles with a cubic cleavage, one of the main structural characteristics of galena (Warren

et al.,1987). The EDX spectra (Figure 3 (b)) confirmed that the galena ore was mainly comprised of lead (Pb) and sulfur (S). The analysis also revealed traces of oxygen (O) in the feed sample, suggesting some degree of oxidation of galena surfaces, possibly attributed to the air exposure of the sample while being dry-ground.

3.3 Zeta Potential Analysis and the Chemisorption Models

The measured and calculated zeta potentials versus pH for a galena particle conditioned in 0.5, 1, 5, 10 and 100 mM NaCl solutions are presented in Figure 4.

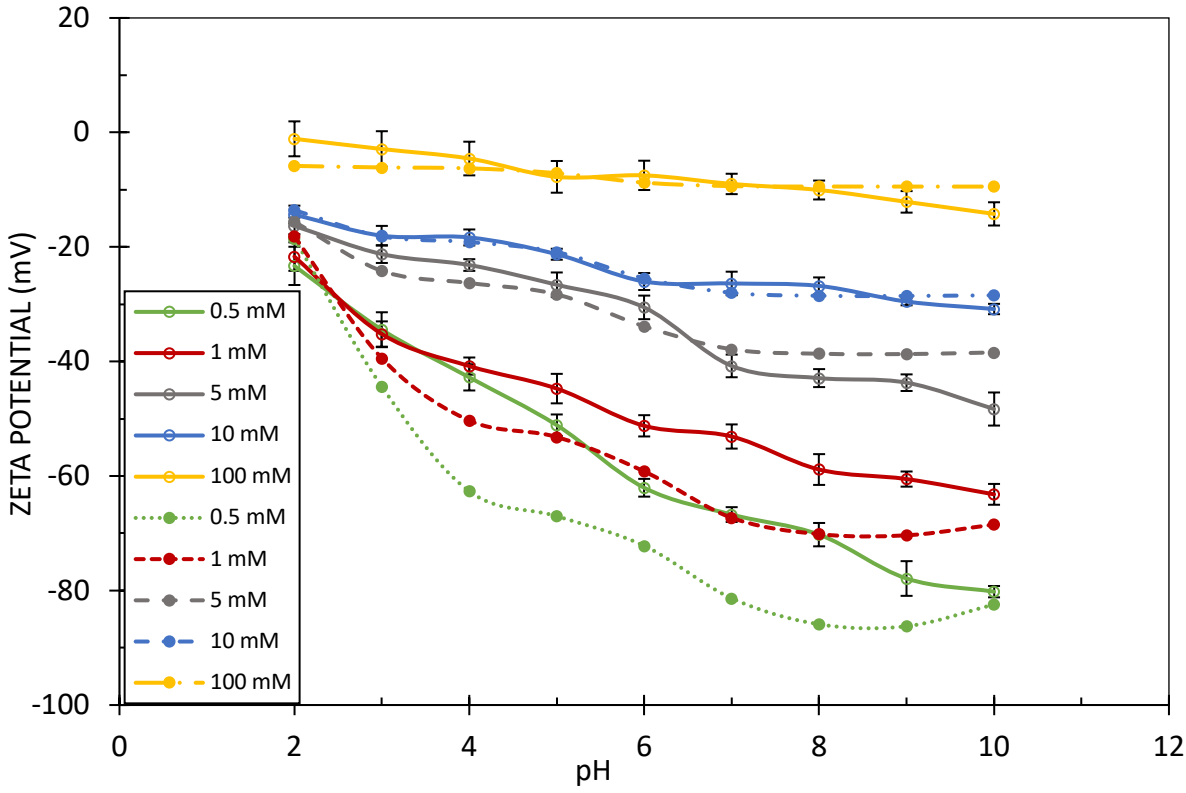

Figure 4. Zeta potential versus pH curves for galena conditioned in 0.5, 1, 5, 10 and 100 mM NaCl solutions. Solid lines represent the measured values, dashed lines illustrate the calculated values using the galena chemisorption model. The error bars represent the standard error of the mean.

The measured zeta potentials of galena conditioned in NaCl solutions decreased from -1 to -82 mV as the pH increased. These zeta potential values were always negative indicating the

isoelectric point (IEP) is at pH < 1. A number of researchers have observed the surface of galena to be negatively charged over most pH values, while others reported the (IEP) of galena to occur between pH 2-8. These discrepancies in the reported (IEP) values could be attributed to the complexity of oxidation of sulfide minerals (Pugh,1988). The value of the isoelectric point (IEP) is, therefore, often used to represent the level of oxidation of the sulfide mineral, where a low (IEP) indicates a surface which is less oxidised, while a high (IEP) suggest heavy oxidation (Das,2006). A low (IEP) of galena, reported in this study, could be attributed to the surface coating of elemental sulfur (S^0) produced by the following:

$$\mathrm{MS} \rightarrow \mathrm{M^{2+}} + \mathrm{S^0} + 2\mathrm{e}\ (\text{oxidation}) \text{ and} \tag{25}$$

$$\frac{1}{2}\mathrm{O_2} + 2\mathrm{H^+} + 2\mathrm{e} \rightarrow \mathrm{H_2O} \text{ or} \tag{26}$$

$$2\mathrm{H_2O} + 2\mathrm{e} \rightarrow \mathrm{H_2} + 2\mathrm{OH^-}\ (\text{reduction}) \tag{27}$$

The oxidation of galena will result in the formation of both the elemental sulfur (S^0) and a metal ion (Healy and Moignard,1976). Our measured zeta potentials of galena are consistent with the previously reported galena zeta potentials, indicating that a non-oxidized galena surface will be negatively charged, with the zeta potentials values close to that of elemental sulfur. Once oxidized, the zeta potential versus pH curves will become less negative due to the increased metal oxide/hydroxide species covering the surface of the mineral (Wang et al.,2017).

Figure 4 shows that the zeta potentials of galena were more negative at lower NaCl concentrations, and as the NaCl concentration was increased, the zeta potentials became less negative. A more negative zeta potential value indicates that the colloidal stability of galena particles is greater for the lower NaCl concentrations (ie. 0.5 mM), meaning that the particles are less likely to form aggregates in this solution compared to a 100 mM NaCl solution. An increase in NaCl concentration causes a reduction in the Debye length and the ionic diffuse layers between the particle and the solution, and as the magnitude of the zeta potential decreases, the particles tend to agglomerate. The increased repulsion indicated by the more negative zeta potentials at the lower NaCl concentrations will also prevent galena particles from attaching onto the air bubbles, decreasing flotation efficiency (Huo et al.,2019). On the other hand, for increased pH, the $\mathrm{H^+}$ concentration in solution decreases, while the cation

312 (Na^+) and the anion (Cl^-) concentrations remain unaffected. The calculations of the
313 chemisorption model for galena and the measured negative zeta potentials suggest that the
314 charge on the surface of galena is mainly regulated by the anions present in the system. The
315 equilibrium constant for the direct binding of the anion (pK_{Cl}) has a value of 7.911 which is
316 higher than the other constants in the model (Table 1).

317 Figure 5 shows the measured and calculated zeta potentials versus pH for an air bubble
318 conditioned in 1 and 10 mM NaCl solutions.

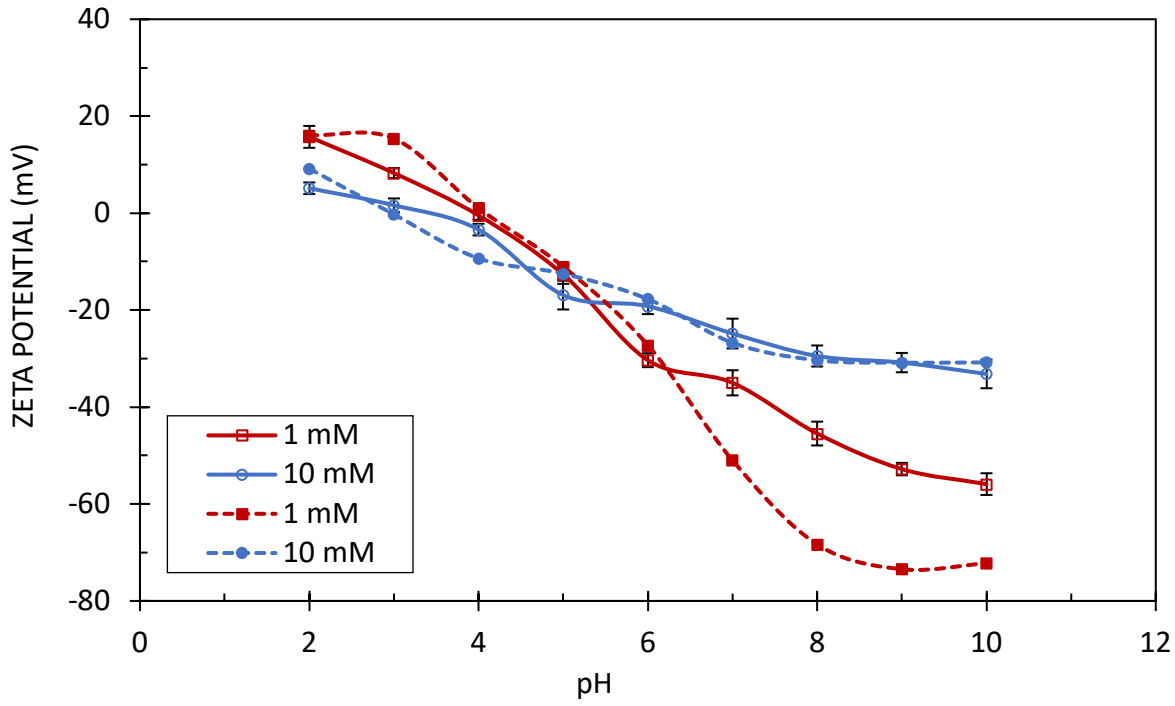

Figure 5. Zeta potential versus pH curves for air bubble conditioned in 1mM and 10mM of NaCl solution. Solid lines represent the measured values (Yang et al.,2001), dashed lines illustrate the calculated values using the bubble chemisorption model. Error bars represent the standard error of the mean.

319 In an aqueous solution, an ionic diffuse layer will also form around an air bubble. Leroy et
320 al.,2012 reported the (IEP) of a bubble to be around pH 3.8. For example, Oliveira and
321 Rubio,2011, have found that a bubble carries a negative charge for pH of 2 or greater when
322 immersed in salt solutions. There have also been reports of the zeta potential of an air bubble

decreasing with increasing ionic concentration, suggesting limited adsorption of Na^+ and Cl^- ions near the gas/water interface (Li and Somasundran,1992).

Figure 5 presents data from Yang et al.,2001 for the calculated and measured zeta potentials of an air bubble in NaCl solutions of different concentrations, as a function of solution pH. This shows that an air bubble is positively charged at pH 2-3, with the exact value depending on the NaCl concentration. Bueno-Tokunga et al.,2015 also measured the zeta potential of an air bubble in an aqueous solution at pH around 2 and found that in an acidic environment the bubble will carry a positive charge. According to Pineres and Barraza,2011, these positive zeta potentials at lower pH may be due to acid formation. The negative zeta potential values in the alkaline range (pH > 7) could be attributed to a higher number of OH^- ions compared to H^+ ions in the air/water interfaces. Yoon and Yordan,1988 proposed that this difference in ion concentration might be related to the difference in enthalpies of hydration between OH^- ions (-446.8 kJ/mol) and H^+ ions (-1104 kJ/mol). There has, however, been an ongoing debate on the nature of interactions at the air/water interface (Beattie et al.,2009).

3.4 Micro-Flotation Experiments

The objective of the micro-flotation experiments was to investigate the effects of NaCl on the galena recovery in the flotation process. The results from micro-flotation experiments are presented in Figure 6.

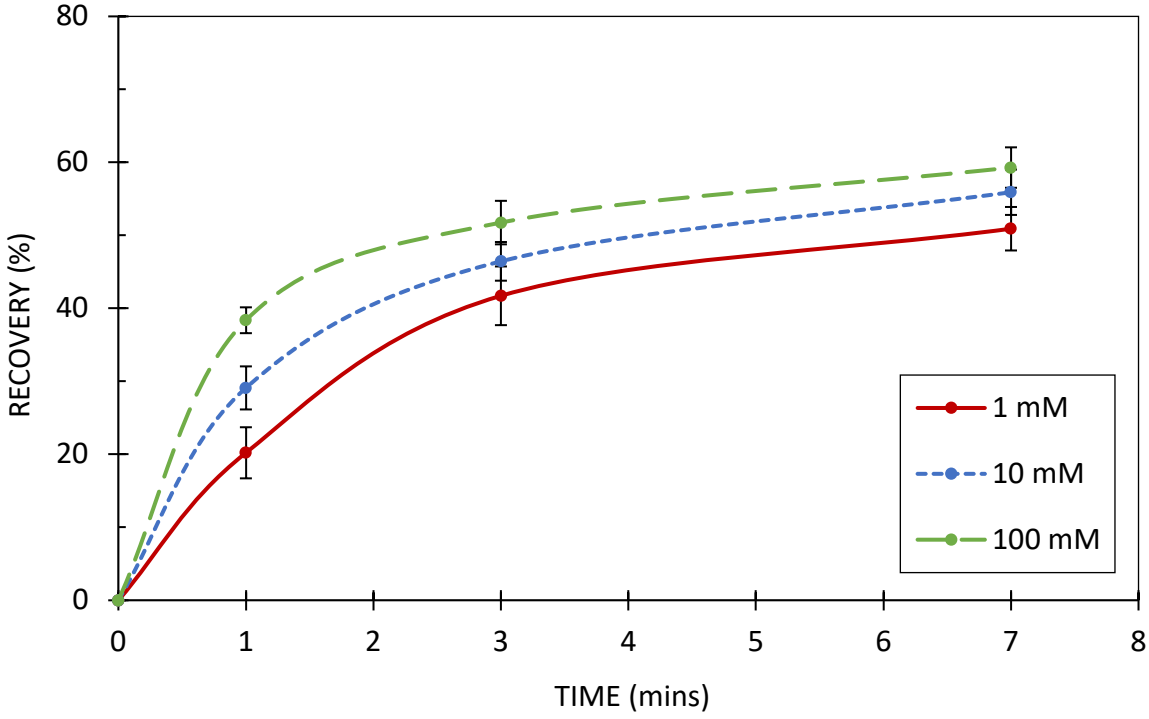

Figure 6. Recovery of galena at pH 9 as a function of flotation time at different ionic concentrations. Error bars indicate a standard error of the mean values.

From the results in Figure 6, it can be seen that the recovery of galena increased with increasing NaCl concentration. At 7 minutes, the recovery for the solution containing 1 mM NaCl was around 50%, compared to ~59% for the 100 mM NaCl solution. The most significant differences in total galena recovery were observed within the first minute of the flotation tests, where recovery for the solution with 1 mM was ~20%, compared to ~29% for the 10 mM solution and ~ 38.5% for the 100 mM NaCl solution (Figure 6). A possible explanation for the higher galena recoveries as salt addition is increased might be related to the induction time, which is described by Nguyen and Schulze,2004, as the time needed for the intervening liquid film to drain to the critical thickness for the formation of a stable particle-bubble aggregate. In more concentrated electrolytes, the repulsion between a particle and an air bubble will decrease, in turn decreasing the water film stability. Consequently, the time required for the intervening film to rupture will decrease, leading to a faster particle-bubble attachment and recovery. The observed higher recoveries of the flotation tests in NaCl solutions can also be attributed to the

compression of the ionic diffuse layers and an enhanced particle aggregation when the repulsive forces are reduced (Wang and Peng,2014).

According to Jeldres et al.,2016, the addition of salt ions will affect the mobility of the water molecules in salt solutions, by reducing the surface hydration. The adsorption of salt ions on the surface of the particle will disrupt of the hydration layers surrounding the particle, giving rise to stronger attractive forces between a particle and an air bubble (Klassen and Mokrousov,1963).

A possible reason for increased galena recovery at higher NaCl concentrations could also be related to the air bubbles themselves. In a flotation process, frothers are often added to the pulp to stabilize the froth and assist in the reduction of bubble coalescence (Ramos et al.,2013). On a par with a frother, the addition of NaCl has been reported to be beneficial to the process, assisting with froth stabilization as well as reducing the bubble size (Castro et al.,2013; Quinn et al.,2014). During flotation, a smaller bubble size is more favourable as it leads to increased collision and attachment efficiencies, resulting in an increased mineral recovery (Dobby and Finch,1986). According to Craig et al.,1993b, a reduction in the bubble size at higher ionic concentration can be attributed to the fact that when inorganic salt ions are added to water, they seem to slow the inner-bubble drainage, thereby promoting the stability in the froth phase. The addition of salt ions has been shown to inhibit bubble coalescence by increasing the contact area and the attachment efficiency between the particle and air bubble (Wu et al.,2016; Craig et al.,1993a; Craig et al. 1993b; Klassen and Mokrousov,1963). The foam stability will increase as the dynamic processes involved in the thinning and rupture of the intervening film are altered due to the increased salt concentration. Likewise, Zhang et al.,2008 suggested that increasing solution salinity decreases gas solubility in the solution, causing air precipitation on the mineral surfaces and leading to the formation of nano-bubbles. These nano-bubbles have been shown to enhance the interactions between particles and bubbles, by improving the attachment efficiency and consequently the recovery (Calgaroto et al.,2014).

3.5 Total Interaction Free Energy

The calculated total interaction free energies between a galena particle and an air bubble in solutions containing increasing concentrations of NaCl, at pH 9, are illustrated in Figure 7.

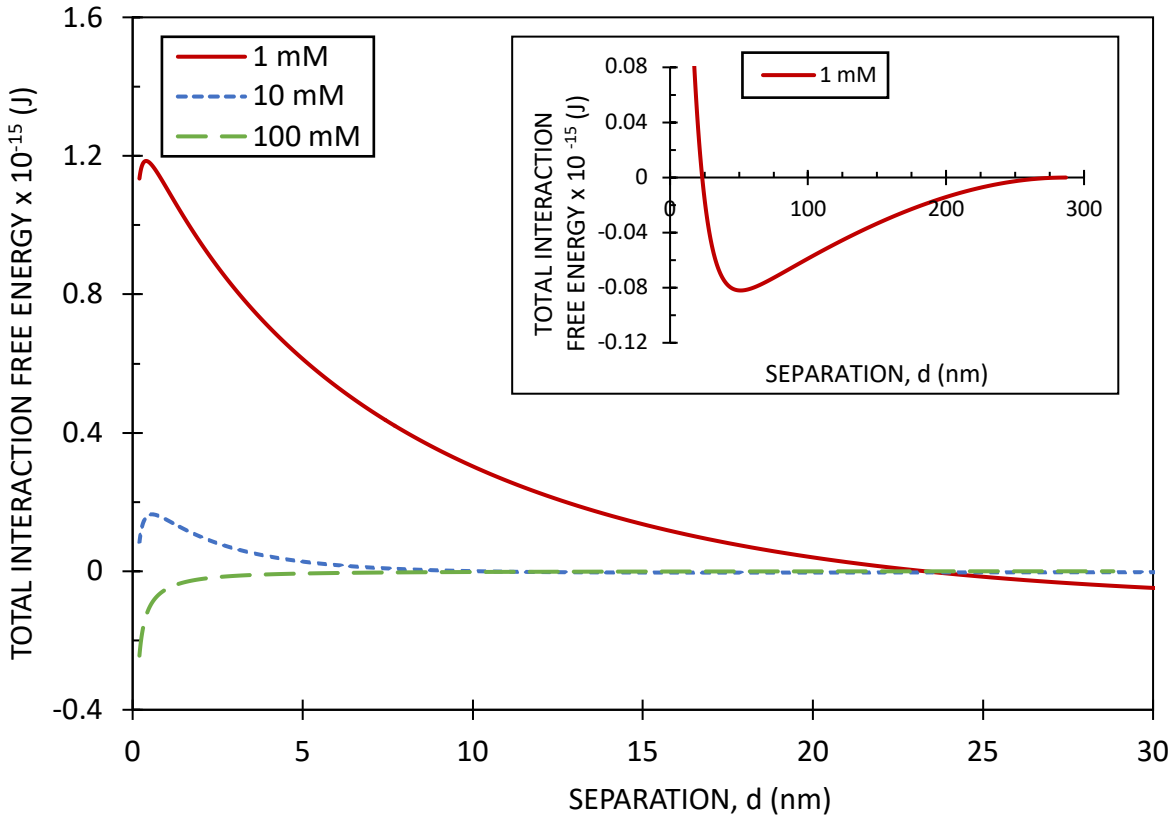

Figure 7. The total interaction free energy versus separation distance between galena and an air bubble in 1, 10 and 100 mM NaCl solutions, at pH 9. 40μm and 1000μm were used as the particle and bubble radii, respectively. The inset shows the secondary minimum of the galena/air bubble interaction in 1 mM NaCl solution, at pH 9, appearing at larger (>25 nm) separation distances.

In Figure 7, the energy profile for 1 mM NaCl showed an energy barrier of 1.2 x 10^{-15} J at around 0.5 nm separation. An energy barrier appears when repulsion exceeds attraction. At lower concentrations strong repulsion dominates the interactions at shorter separation distances. At a distances of > 25 nm, however, a secondary minimum was observed in the 1 mM energy profile, illustrated in the inset in Figure 7. This secondary minimum represents a metastable equilibrium between galena and an air bubble where attraction, although weak, dominates the interactions. This attraction at the secondary minimum is not enough to guarantee a stable

392 galena/air bubble aggregation, however. The repulsive barrier between the particles and air
393 bubbles, depicted in the 1 mM energy curve in Figure 7, causes them to redisperse.

394 The energy profile for 10 mM NaCl also exhibits a repulsive maximum, but with a significantly
395 smaller energy barrier of 0.1 x 10^{-15} J at around 0.5 nm separation. The calculated Debye lengths
396 (κ^{-1}) in 1 mM, 10 mM and 100 mM NaCl concentrations were 9.62 nm, 3.04 nm and 0.96 nm,
397 respectively. As the ionic concentration increases, the Debye lengths decrease and so do the
398 heights of the energy barriers. A lower energy barrier allows the particle and bubble to come
399 closer together, with significantly less kinetic energy required to form an attachment, resulting
400 in an increased particle recovery, which is seen in Figure 6.

401 The total interaction free energy between a galena particle and an air bubble in 100 mM
402 solution is always negative and monotonically varying with the separation distance. This
403 increased attraction was largely attributed to the screening of the particle and bubble ionic
404 diffuse layers such that the total interaction is mainly controlled by the attractive van der Waals
405 interactions. The nature of this repulsion/attraction transition is discussed in more detail in a
406 study by Trefalt et al.,2016, where this transition was shown to strongly depend on the value of
407 the charge regulation parameter.

408 In the DLVO description of the system, it is not possible to vary the attractive component of the
409 interaction energy, as this value is fixed by the Hamaker constant of the interacting materials.
410 However, the degree of repulsion can be reduced by adding more ions to the system thereby
411 decreasing the screening length resulting from an increased ionic strength. The higher the salt
412 concentration in solution, the shorter the Debye length, meaning a shorter range of repulsion
413 from the ion adsorption layers. Decreasing the ionic repulsion will increase the attachment
414 efficiency and result in a higher galena recovery. At the 1 mM NaCl concentration, the efficiency
415 of particle-bubble attachment is decreased by greater repulsion between galena and an air
416 bubble, arising from stronger counterion adsorption in accordance with the more negative
417 zeta potentials measured for galena (Figure 4) and an air bubble (Figure 5) at this
418 concentration. Possibly due to the long-range nature of the ionic diffuse layer forces compared
419 to the shorter-range van der Waals interactions, the efficiency of flotation at ionic
420 concentrations smaller than 10 mM was predominantly controlled by these ionic diffuse layer

forces. Our micro-flotation results indicated that particles and bubbles could form aggregates even at low NaCl concentrations suggesting that their kinetic energies were enough to overcome the energy barrier arising due to the repulsive ionic diffuse layer interactions, possibly aided by the existence of the secondary minimum. Due to screening of the electrostatic repulsive forces in 100 mM NaCl solution, the total interactions then become mainly dominated by the attractive van der Waals forces.

In this study, we evaluated the interaction free energy between a galena particle and an air bubble under conditions of charge regulation. An alternative "approximate" analytical method which is frequently employed and uses constant potential conditions, calculates the total interaction energy $(\mathbf{E_{DLVO}})$ as:

$$\mathrm{E_{DLVO}} = \mathrm{E_{vdW}} + \mathrm{E_{el}} \tag{28}$$

1. van der Waals interactions $(\mathbf{E_{vdW}})$

$$\mathrm{E_{vdW}} = -\frac{\mathrm{A_{132}R_pR_b}}{6\mathrm{d}\left(\mathrm{R_p}+\mathrm{R_b}\right)} \tag{29}$$

where $\mathbf{d}$ is the surface to surface distance, $\mathbf{R_p}$ and $\mathbf{R_b}$ are the particle and bubble radii, respectively, and $\mathbf{A_{132}}$ is the Hamaker constant.

2. Electrostatic (ionic) interactions $(\mathbf{E_{el}})$

$$\mathrm{E_{el}} = 4\pi\varepsilon_0\varepsilon_\mathrm{r}\frac{\mathrm{D_pD_b}}{2\left(\mathrm{D_p}+\mathrm{D_b}\right)}\left[\psi_\mathrm{p}\psi_\mathrm{b}\mathrm{e}^{-\kappa\mathrm{H}} - \frac{1}{4}\left(\psi_\mathrm{p}^2+\psi_\mathrm{b}^2\right)\mathrm{e}^{-2\kappa\mathrm{H}}\right] \tag{30}$$

where $\boldsymbol{\varepsilon_r}$ is the dielectric constant, $\boldsymbol{\varepsilon_0}$ is the dielectric permittivity of the medium in vacuum, $\boldsymbol{\kappa}$ is the reciprocal of the Debye length, and $\boldsymbol{\psi_p}$ and $\boldsymbol{\psi_b}$ are the particle and bubble surface potentials, respectively and $\mathbf{D_p}$ and $\mathbf{D_b}$ are the particle and bubble diameters, respectively.

Figure 8 compares the total interaction energy $(\mathbf{E_{DLVO}})$ calculated by the "approximate" method (constant potential) against the total interaction free energy $(\mathbf{F_{tot}})$ under charge regulated conditions between a galena particle and an air bubble in different NaCl concentrations, at pH 9. The radii of the galena particle and air bubble radii were 40µm and 1000µm, respectively.

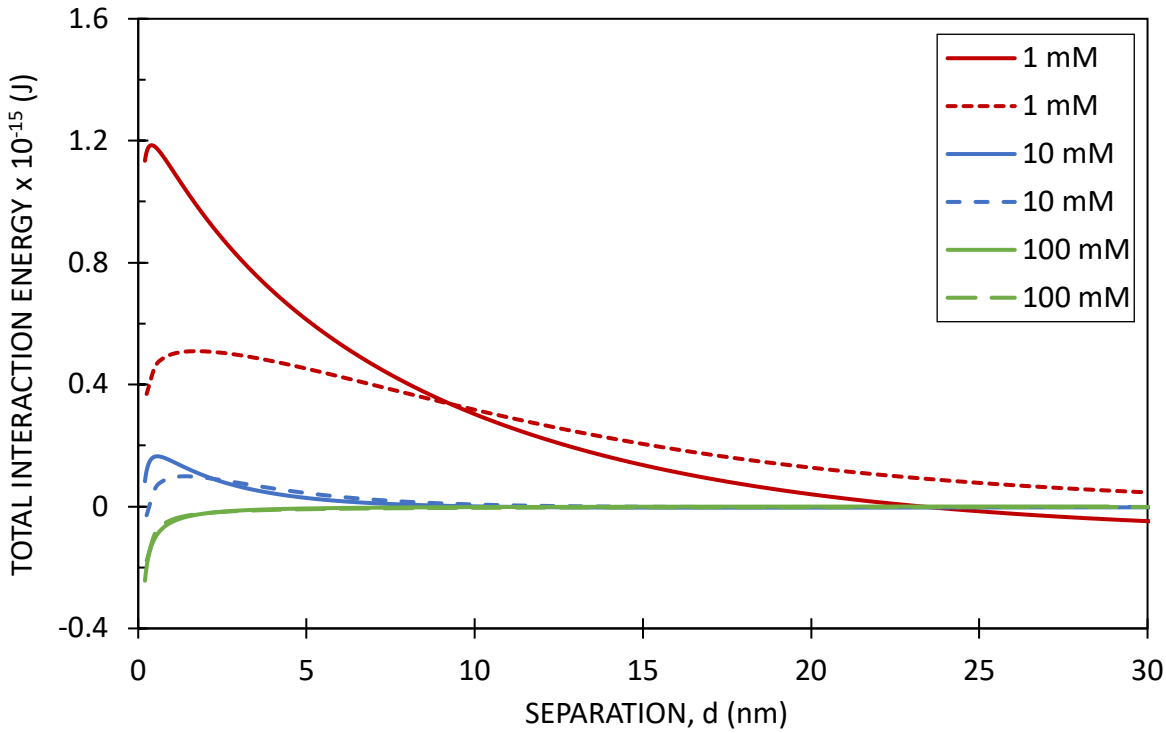

Figure 8. The total interaction free energy (solid lines)-calculated using Eq.(12), and the total interaction energy E_{DLVO} (dashed lines)-calculated using Eq.(28), versus distance of separation between a galena particle and an air bubble in 1, 10 and 100 mM NaCl solutions, at pH 9.

When we compare the results produced by the two methods against each other (energy curves in Figure 8), the results are not entirely consistent. The major discrepancy between the methods is noticed in the lowest NaCl concentration curves. Indeed, both profiles representing the interactions in 1 mM indicate an energy barrier, but the height of this barrier calculated using Eq.(12) was roughly double the height of the one calculated using the "approximate" method represented by Eq.(28) with the repulsion extending over a distance of about one Debye length. As mentioned earlier, the van der Waals contribution to the total interaction energy mainly depends on a Hamaker constant value, specific to that interaction. Changes to ionic concentrations will have no effect on the van der Waals interactions. For this reason, we should focus on comparing how the electrostatic (ionic) interactions are represented and calculated in each method. In the expression for the electrostatic (ionic) interactions described by Eq.(30), the surface potentials for a particle and an air bubble remain constant, they do not

455 change despite the changes in the separation distance. Consequently, the “approximate”
456 method can be identified as a “constant potential” method. On the other hand, when we
457 calculate the total interaction free energy using Eq.(12), we are taking into consideration the
458 varying particle and bubble surface potentials. We note that these surface potential variations
459 result from the changes in the concentration and the distributions of ions inside the diffuse
460 layer. Subsequently, this method can be identified as a “charge-regulated potential” method.

461 One of the main objectives of this study involved studying the contributions due to the specific
462 ion binding activities at surface sites, which are represented by the term $\mathbf{F_{chem}}$ in Eq.(12), one
463 of the four individual components to the total interaction free energy calculations whose
464 contributions are neglected in the “approximate” analytical method. With this in mind, we
465 postulate that the underestimated energy barrier for the 1 mM energy profile, determined using
466 Eq.(28), resulted from a charge regulation process not being taken into consideration by the
467 $(\mathbf{E_{DLVO}})$ analytical method.

468

469 ## 4. CONCLUSION

470 This work presents new findings of the effects of different NaCl concentrations on the flotation
471 of galena. The micro-flotation tests were carried out at three different NaCl concentrations, at
472 pH 9. It was found that the recovery of galena increased with increased NaCl concentration.

473 Chemisorption models describing the local surface charge at the galena/electrolyte and
474 bubble/electrolyte interface have been identified and applied. Chemisorption parameters
475 were calibrated against the measured zeta potentials. The predicted zeta potential values were
476 in line with the measured zeta potentials.

477 The total interaction free energy between a galena and an air bubble for each of the three NaCl
478 concentrations tested in this study was determined using the DLVO theory with surface charge
479 determined based on the identified chemisorption model parameters. The repulsive forces
480 were shown to dominate at a NaCl concentration of 1 mM, with a well-defined energy barrier
481 at a particle-bubble separation distance of 0.5 nm. On the other hand, the galena/air bubble
482 interactions in 10 mM NaCl solution were controlled by a significantly weaker ionic diffuse layer

repulsions, indicated by a lower energy barrier as a result of an increase in NaCl concentration in solution. The total energy calculated in 100 mM NaCl concentration suggested interactions which are predominantly controlled by the attractive van der Waals forces. The theoretical models appeared to be in agreement with the micro-flotation recovery results, recognising that they may be useful in predicting the flotation behaviour of galena.

The main focus of this study was to gain a better understanding of the effects of NaCl addition on galena recovery in flotation. Future work will involve experiments with an addition of a collector, as well as investigations into the effects of other salt ions on the flotation of galena.

5. REFERENCES

Alnæs, M., Blechta, J., Hake, J., Johansson, A., Kehlet, B., Logg, A., Richardson, C., Ring, J., Rognes, M.E. and Wells, G.N. The FEniCS Project Version 1.5. Archive of Numerical Software, Vol.3 No.100, 2015.

Beattie, J.K., Djerdjev, A.M. and Warr, G.G. (2009). The surface of neat water is basic. *Faraday Discussions* ***141,*** 31-39.

Bergström, L. (1997). Hamaker constants of inorganic materials. *Advances in Colloid and Interface Science* ***70,*** 125-169.

Bueno-Tokunga, A., Perez-Garibay, R. and Martinez-Carrillo, D. (2015). Zeta potential of air bubbles conditioned with typical froth flotation reagents. *International Journal of Mineral Processing* ***140,*** 50-57.

Calgaroto, S., Wilber, K.Q. and Rubio, J. (2014). On the nanobubbles interfacial properties and future applications in flotation. *Minerals Engineering* ***60,*** 33-40.

Castro, S., Miranda, C., Toledo, P. and Laskowski, J.S. (2013). Effect of frothers on bubble coalescence and foaming in electrolyte solutions and seawater. *International Journal of Mineral Processing* ***124,*** 8-14.

508 Craig, V.S.J., Ninham, B.W. and Pashley, R.M. (1993a). Effect of electrolytes on bubble
509 coalescence. *Nature* ***364*** *(6435),* 317-319.

510 Craig, V.S.J., Ninham, B.W. and Pashley, R.M. (1993b). The effect of electrolytes on bubble
511 coalescence in water. *The Journal of Physical Chemistry* ***97*** *(39),* 10192-10197.

512 Dagastine, R.R., Prieve, D.C. and White, L.R. (2000). The dielectric function for water and its
513 application to van der Waals forces. *Journal of Colloid and Interface Science* ***231***, 351-
514 358.

515 Das, K.K. (2006). Electrokinetics of mineral particles. In Encyclopedia of Surface and Colloid
516 Science. 2nd Ed. Columbia University, New York, USA.

517 Derjaguin, B. (1934). Untersuchungen über die Reibung und Adhäsion, IV. *Kolloid-Zeitschrift* ***69***,
518 155-164.

519 Derjaguin, B.V. and Landau, L. (1941). Theory of the stability of strongly charged lyophobic sols
520 and of the adhesion of strongly charged particles in solution of electrolytes. *Acta*
521 *Physicochim. USSR* ***14,*** 633-662.

522 Dobby, G.S. and Finch, J.A. (1986). Particle collection in columns-Gas rate and bubble size
523 effects. *Canadian Metallurgical Quarterly* ***27,*** 85-90.

524 Fornasiero, D., Li, F. and Ralston, J. (1993). Oxidation of galena II. Electrokinetic Study. *Journal*
525 *of Colloid and Interface Science* ***164,*** 345-354.

526 Healy, T.W. and Moignard, M.S. (1976). A review of electrokinetic studies of metal sulfides. In
527 Flotation-A.M. Gaudin Memorial Volume; Fuerstenau, M.C. Ed; AIME: New York, Vol 1,
528 275-297.

529 Hencer, M., Celik, M.S. and Miller, J.D. (2001). The significance of interfacial water structure in
530 soluble salt flotation systems. *Journal of Colloid and Interface Science* ***235,*** 150-161.

531 Huo, W., Zhang, X., Gan, K., Chen, Y., Xu, J. and Yang, J. (2019). Effect of zeta potential on
532 properties of foamed colloidal suspension. *Journal of the European Ceramic Society* ***39,***
533 574-583.

534 Jeldres, R.I., Forbes, L. and Cisternas, L.A. (2016). Effect of Seawater on Sulfide Ore Flotation: A
535 review. *Mineral Processing and Extractive Metallurgy Review* ***37*** *(6),* 369-384.

536 Klassen, V.I. and Mokrousov, V.A. (1963). An introduction to the theory of flotation.
537 Butterworths, London.

538 Lee, S. and Sigmund, W.M. (2002). AFM study of repulsive van der Waals forces between Teflon
539 AF™ thin film and silica or alumina. *Colloids and Surfaces A: Physicochemical and*
540 *Engineering Aspects* ***204,*** 43-50.

541 Leroy, P., Jougnot, D., Revil, A., Lassin, A and Azaroual, M. (2012). A double-layer model of the
542 gas bubble/water interface. *Journal of Colloid and Interface Science* ***388,*** 243-256.

543 Li, C. and Somasundaran, P. (1992). Role of the electrical double layer forces and
544 hydrophobicity in coal flotation in NaCl solutions. *Energy and Fuels* ***7*** *(2),* 244-248.

545 Lucay, F., Cisternas, L.A., Galvez, E.D. and Lopez-Valdivieso, A. (2015). Study of the natural
546 floatability of molybdenite fines in saline solutions. Effect of gypsum precipitation.
547 *Minerals and Metallurgical Processing Journal* ***32,*** 203-208.

548 Nguyen, A.V. and Schulze, H.J. (2004). Colloidal Science of Flotation. New York, Marcel Dekker.

549 Oliveira, C. and Rubio, J. (2011). Zeta potential of single and polymer-coated microbubbles
550 using an adapted microelectrophoresis technique. *International Journal of Mineral*
551 *Processing* ***98*** *(1-2),* 118-123.

552 Parsons, D.F. and Ninham, B.W. (2012). Nonelectrostatic ionic forces between dissimilar
553 surfaces: A mechanism for colloid separation. *The Journal of Physical Chemistry C* ***116***,
554 7782-7792.

555 Parsons, D.F. and Salis, A. (2015). The impact of the competitive adsorption of ions at surface
556 sites on surface free energies and surface forces. *The Journal of Chemical Physics* ***142****.*

557 Parsons, D.F. and Salis, A. (2019). A thermodynamic correction to the theory of competitive
558 chemisorption of ions at surface sites with nonelectrostatic physisorption. *The Journal*
559 *of Chemical Physics* ***151****.*

560 Pineres, J. and Barraza, J. (2011). Energy barrier of aggregates coal particle-bubble through the
561 extended DLVO theory. *International Journal of Mineral Processing* ***100,*** 14-20.

562 Pugh, R.J. (1988). Surface chemical studies on sulphide flotation. Proceedings of XVI
563 International Mineral Processing Congress, Stockholm, June 5-10; Forssberg, E., Ed.;
564 Elsevier: Amsterdam, 751.

565 Quinn, J.J., Kracht, W., Gomez, C.O., Gagnon, C. and Finch, J.A. (2014). Comparing the effect of
566 salts and frother (MIBC) on gas dispersion and froth properties. *Minerals Engineering* ***20,***
567 1296-1302.

568 Ramos, O., Castro, S. and Laskowski, J.S. (2013). Copper-molybdenum ores flotation in
569 seawater: floatability and frothability. *Minerals Engineering* ***53,*** 108-112.

570 Smith, A.M., Lee, A.A. and Perkin, S. (2016). The electrostatic screening length in concentrated
571 electrolytes increases with concentration. *Journal of Physical Chemistry Letters* ***7,*** 2157-
572 2167.

573 Smith, L.K. and Heyes, G.W. (2012). The effect of water quality on the collector-less flotation of
574 chalcopyrite and bornite. *Third International Congress on Water Management in the*
575 *Mining Industry,* Santiago, Chile.

576 Takagishi, H., Masuda, T., Shimoda, T., Maezono, R. and Hongo, K. (2019). Method for the
577 calculation of the Hamaker constants of organic materials by the Lifshitz macroscopic
578 approach with Density Functional Theory. *The Journal of Physical Chemistry* ***123,*** 8726-
579 8733.

580 Trefalt, G., Behrens, S.H. and Borkovec, M. (2016). Charge regulation in the Electrical Double
581 Layer: Ion adsorption and surface interactions. *Langmuir* ***32,*** 380-400.

582 Verwey, E.J.W. and Overbeek, J.T.G. (1948). Theory of stability of Lyophobic Colloids. Elsevier,
583 Amsterdam.

584 Wang, B. and Peng, Y. (2014). The effect of saline water on mineral flotation – a critical review.
585 *Minerals Engineering* ***66-68,*** 13-24.

586 Wang, D., Jiao, F., Qin, W. and Wang, X. (2017). Effect of surface oxidation on the flotation
587 separation of chalcopyrite and galena using sodium humate as depressant. *Separation*
588 *Science and Technology* ***53****, 961-972.*

589 Warren, G.W., Kim, S.H. and Henein, H. (1987). The effect of chloride ion on the ferric chloride
590 leaching of galena concentrate. *Metallurgical Transactions B* ***18****,* 59-69.

591 Wu, Z., Wang, X., Liu, H., Zhang, H. and Miller, J.D. (2016). Some physicochemical aspects of
592 water-soluble mineral flotation. *Advances in Colloid and Interface Science* ***235****,* 190-200.

593 Yang, C., Dabros, T., Li, D., Czarnecki, J. and Masliyah, J.H. (2001). Measurement of the Zeta
594 Potential of Gas Bubbles in Aqueous Solutions by Microelectrophoresis. *Journal of*
595 *Colloid and Interface Science* ***243****,* 128-135.

596 Yoon, R. and Yordan, J. (1988). Zeta potential measurement on microbubble generated using
597 various surfactants. *Journal of Colloid and Interface Science* ***113****,* 430-438.

598 Zhang, X.H., Quinn, A. and Ducker, W.A. (2008). Nanobubbles at the interface between water
599 and hydrophobic solid. *Langmuir* ***24****,* 4756-4764.